Thesis
H9574

T145103

ON THE COMPRESSIVE BUCKLING OF RECTANGULAR PLATES WITH ADVANCED-COMPOSITE-REINFORCED, CENTRAL LONGITUDINAL STIFFENERS

A THESIS

SUBMITTED TO THE DEPARTMENT OF AERONAUTICS AND ASTRONAUTICS

AND THE COMMITTEE ON GRADUATE STUDIES

OF STANFORD UNIVERSITY

IN PARTIAL FULFILLMENT OF THE REQUIREMENTS

FOR THE DEGREE OF

ENGINEER

By

Jerry Francis Huss

November 1971

H 9574

ACKNOWLEDGEMENT

The author wishes to express his sincere gratitude to Professor Jean Mayers for his advice, instruction, and encouragement during the course of this investigation. Appreciation is also extended to the United States Navy and the U.S. Naval Postgraduate School for the time and financial aid which made this investigation and study at Stanford University possible. Special thanks are due to Professor Charles H. Kahr of the Naval Postgraduate School Faculty without whose encouragement and confidence this opportunity for study would not have been possible.

Finally, the author wishes to thank his wife, Judy, for her support and encouragement throughout the span of this project.

SUMMARY

A theoretical investigation is undertaken to study the buckling of a thin, rectangular, homogeneous, isotropic flat plate augmented with a centrally located longitudinal stiffener. The influence on overall plate efficiency of the use of advanced composite materials in the stiffener is developed and discussed. Results of the analysis are presented in the form of charts to demonstrate the effects of fibrous-composite reinforcement of the stiffener on the critical-stress-to-weight ratio of the plate.

TABLE OF CONTENTS

	Page
ACKNOWLEDGEMENT	iii
SUMMARY	iv
LIST OF ILLUSTRATIONS	vi
LIST OF SYMBOLS	vii
INTRODUCTION	1
GENERAL THEORY	4
Strain-Displacement Relations	4
Stress-Strain Relations	4
Potential Energy	5
Variational Principle and Governing Equations	7
METHOD OF SOLUTION	9
General Case	9
Homogeneous, Isotropic Square Plate	11
RESULTS AND DISCUSSION	14
CONCLUDING REMARKS	17
REFERENCES	19
APPENDIXES	
I. Development of Buckling Criterion	20
II. Determination of Equivalent Values of (EI) and (GJ) in Composite-Reinforced Stiffener	25
FIGURES	27

LIST OF ILLUSTRATIONS

Figure		Page
1	Geometry of Homogeneous, Isotropic Plate With Longitudinal Stiffener	27
2	Buckling Efficiency Curve for Aluminum Plate With Longitudinal Stiffener Augmented With Varying Percentage (by Volume) of Graphite Epoxy	28
3	Buckling Efficiency Curve for Aluminum Plate With Longitudinal Stiffener Augmented With Varying Percentage (by Volume) of Graphite Epoxy ($G_{comp} = G_{base}$)	29
4	Buckling Efficiency Curve for Aluminum Plate With Longitudinal Stiffener Augmented With Varying Percentage (by Volume) of Boron Epoxy	30
5	Buckling Coefficient Curve for Aluminum Plate With Aluminum Longitudinal Stiffener	31
6	Geometry of the Transformation of a Composite Beam Into an Equivalent Beam of one Material	32

LIST OF SYMBOLS

A_{mn}	arbitrary constant in lateral deflection function, in.
(A_s)	cross-sectional area of longitudinal stiffener, $in.^2$
b	width of flat plate, in.
D	flexural stiffness of homogeneous, isotropic plate, lb-in.
D_x, D_y	flexural stiffnesses of orthotropic plate in axial and chordwise directions, respectively, lb-in.
D_{xy}	torsional stiffness of orthotropic plate, lb-in.
E	Young's modulus of homogeneous isotropic plate and stiffener, $lb/in.^2$
E_x, E_y	extensional stiffenesses of orthotropic plate in axial and chordwise directions, respectively, lb/in.
(EI)	effective flexural stiffness of composite-reinforced stiffener, $lb\text{-}in.^2$
G	shear modulus of homogeneous isotropic plate and stiffener, $lb/in.^2$
G_{xy}	shear stiffness of orthotropic plate, lb/in.
(GJ)	effective torsional stiffness of composite-reinforced stiffener, $lb/in.^2$
h	stiffener height, in.
I	moment of inertia, $in.^4$
J	torsional stiffness constant, $in.^4$
k	arbitrary nondimensional integer
k_x, k_y	buckling coefficients in axial and chordwise directions, respectively
L	length of flat plate and stiffener, in.

M_x, M_y	plate bending moments in x- and y-directions, respectively, lb-in.
m,n	number of buckling halfwaves in x- and y-directions, respectively
N_x, N_y, N_{xy}	middle surface stress resultants, lb/in.
$\bar{N}_x, \bar{N}_y, \bar{N}_{xy}$	applied load resultants, lb/in.
p	arbitrary nondimensional integer
T	torque, lb-in.
t	plate thickness, in.
u,v,w	displacements of point on middle surface of plate in x-, y-, and z-directions, respectively, in.
U	total strain energy of plate and stiffener, lb-in.
U_p	strain energy of plate, lb-in.
U_s	strain energy of stiffener, lb-in.
V	potential of applied loads, lb-in.
w_1	width of actual stiffener, in.
w_2	equivalent width of composite portion of stiffener, in.
x,y,z	plate coordinates, in.
α	buckle aspect ratio of unstiffened plate
γ	beam twisting strain, in./in.
γ_x, γ_y	transverse shearing strains in x- and y-directions, respectively, in./in.
γ_{xy}	plate shearing strain, in./in.
$\delta( )$	Dirac delta function, 1/in.
δ_{nodd}	Kronecker delta function
ϵ_x, ϵ_y	membrane strains in x- and y-directions, respectively, in./in.
θ	angle of twist, radians

μ	Poisson's ratio for homogeneous isotropic plate
μ_x, μ_y	Poisson's ratios for orthotropic plate in x- and y-directions, respectively
ρ	density, $lb/in.^3$
ρ_{ave}	average density of plate and stiffener, $lb/in.^3$
σ	stiffener middle-surface stress, $lb/in.^2$
σ_x, σ_y	plate membrane stresses in x- and y-directions, respectively, $lb/in.^2$
σ_{cr}	critical stress of plate, $lb/in.^2$
τ	stiffener shear stress, $lb/in.^2$

SUBSCRIPTS

base	pertaining to base material (aluminum)
comp	pertaining to composite material (boron epoxy or graphite epoxy)

INTRODUCTION

The trend to higher performance aircraft in all speed regimes has led designers to seek methods of decreasing the structural weight of aircraft while maintaining or increasing the stress levels on the materials involved. One of the most promising means of accomplishing this objective has been the introduction of advanced composite materials to either augment or replace conventional structural materials (for example, aluminum). One type of composite material consists of the incorporation of high-strength, high-modulus filaments into a compatible matrix. Several material system classes currently of active interest include graphite epoxy, boron epoxy, and metal matrices having metal fibers. As pointed out in Reference 1, design and structures engineers, using composites, have the ability to build directional properties into the structure which, in turn, results in improved efficiency. Weight saved, with its direct effect on the design index of strength/weight, is the most attractive feature of the use of high-performance composites. It has not been uncommon for structures-materials engineers to predict weight reductions of as much as forty percent in total systems weight through the potential use of advanced composites in both primary and secondary structures.

With advanced filamentary composites, increased design flexibility of significant degree exists that is not possible with conventional metal structures. However, as with many new developments, work in the composite field has been primarily empirical, while theory and analysis have lagged somewhat behind. Despite the potential of composites, evidence of their use appears only in the reasonably small structural elements that can be designed by test (for example, stabilizers, wing tips, slats, and rotors). The trial and error procedure, especially with materials of such high performance possibilities as composites, can lead to excessive costs due to both inherent high material costs and eventual appearance of structural behavior neither anticipated nor properly estimated. One such case is presented by Durlofsky and Mayers

in Reference 2. Another such case exists with the use of advanced composites to enhance the buckling efficiency of stiffened plates utilized in the construction of wing, fuselage, and empennage structures of aircraft. Peterson[3] studied the effect of an all-composite stiffener in the reinforcement of a simply supported aluminum plate without considering the possibility of an optimized composite-metal-stiffener combination. His results indicate that some caution must be exercised in using high-performance composites in combination with conventional structural concepts and prediction methods.

Earlier studies of conventional stiffened plates under compression, such as those of Barbré,[4] Seide and Stein,[5] and Gomza and Stein,[6] neglect the effects of torsional stiffness of the stiffener in establishing buckling criteria. The justification offered is usually that the torsional stiffness of the stiffeners is relatively small when compared with the bending stiffness and that vanishingly small torsional stiffness of the stiffeners is consistent with the appearance of buckle nodes at stiffener locations in the chordwise direction. Such justification, of course, is appropriate for the discrete stiffener spacing of low subsonic speed flight vehicles. For the higher speed ranges, stiffeners are more closely spaced and the stiffener torsional stiffness becomes significant in buckling analysis. Thus, the introduction of composite materials into all or part of a stiffener can possess ramifications not evident in the use of conventional materials. For example, although Young's modulus (E) for a composite may be as much as four times greater than that of a structural metal, the shear modulus (G) may be lower by approximately the same factor. Therefore, neglecting torsional rigidity in a composite-metal system with closely spaced stiffeners may introduce unsatisfactory errors in buckling calculations.

It is the purpose of this investigation to (1) present the theory and an approximate analysis for determining the stability of a simply supported, flat, rectangular orthotropic plate with a centrally located,

composite-augmented, longitudinal stiffener and (2) determine for a square plate the effects of varying the percentage (by volume) of composite material in the stiffener with stiffener torsional rigidity included.

GENERAL THEORY

STRAIN-DISPLACEMENT RELATIONS

The strain-displacement relations for small strain, large displacement, and moderate rotation behavior of an orthotropic plate (see Figure 1) can be obtained from Reference 7 as

$$\begin{aligned}
\epsilon_x &= u_{,x} + \frac{1}{2} w_{,x}^2 - z\,(w_{,xx} - \gamma_{x,x}) \\
\epsilon_y &= v_{,y} + \frac{1}{2} w_{,y} - z\,(w_{,yy} - \gamma_{y,y}) \qquad (1) \\
\gamma_{xy} &= u_{,y} + v_{,x} + w_{,x} w_{,y} - 2z\left(w_{,xy} - \frac{\gamma_{x,y}}{2} - \frac{\gamma_{y,x}}{2}\right)
\end{aligned}$$

With a single stiffener buckling into no more than 2 half-wavelengths and a homogeneous, isotropic base plate, however, interlaminar and transverse shear effects become of higher-order significance and they are assumed to be negligible throughout the analysis. Thus, the transverse shear angles γ_x and γ_y are set equal to zero. Further, since buckling is of interest, the stretching of the middle surface of the plate (and stiffener) may be neglected; thus

$$\begin{aligned}
\epsilon_x &= -z w_{,xx} \\
\epsilon_y &= -z w_{,yy} \qquad (2) \\
\gamma_{xy} &= -2z w_{,xy}
\end{aligned}$$

STRESS-STRAIN RELATIONS

For an orthotropic plate in which the stresses do not exceed the elastic limit, Hooke's law is applicable; it is expressed in the following

form relating normal force per unit length of cross section to strain:

$$N_x = \frac{E_x}{1 - \mu_x\mu_y} (\epsilon_x - \mu_y\epsilon_y)$$

$$N_y = \frac{E_y}{1 - \mu_x\mu_y} (\epsilon_y - \mu_x\epsilon_x) \qquad (3)$$

$$N_{xy} = G_{xy}\gamma_{xy}$$

A single longitudinal stiffener possesses the same stress-strain relationships as a one-dimensional beam; that is

$$\sigma = E\epsilon_x$$

$$\tau = G\gamma \qquad (4)$$

POTENTIAL ENERGY

The strain energy stored in an elastic plate of constant thickness due to bending and twisting may be written as

$$U_p = \frac{1}{2t} \int_0^L \int_0^b \int_{-t/2}^{t/2} \left[N_x\epsilon_x + N_y\epsilon_y + N_{xy}\gamma_{xy} \right] dxdydz \qquad (5)$$

Substitution of Equations (2) and (3) into Equation (5) and subsequent integration over the thickness of the plate yields

$$U_p = \frac{1}{2} \int_0^L \int_0^b \left[\frac{D_x}{1 - \mu_x\mu_y} w^2_{,xx} + \frac{D_x\mu_y + D_y\mu_x}{1 - \mu_x\mu_y} w_{,xx}w_{,yy} \right.$$

(Continued)

$$+ \frac{D_y}{1 - \mu_x \mu_y} w^2_{,yy} + 2D_{xy} w^2_{,xy} \Bigg] dxdy \qquad (6)$$

With the use of the Dirac delta function, the potential energy of a single centrally located symmetric longitudinal stiffener (see Figure 1) may be described over the same interval as

$$U_s = \frac{1}{2t} \int_0^L \int_0^b \int_{-h/2}^{h/2} \left[\sigma \epsilon_x + \tau \gamma \right] \delta \left(y - \frac{b}{2} \right) dxdydz \qquad (7)$$

Substitution of Equations (2) and (4) in Equation (7) and subsequent integration over the stiffener height yields

$$U_s = \frac{1}{2} \int_0^L \int_0^b \left[(EI) w^2_{,xx} + (GJ) w^2_{,xy} \right] \delta \left(y - \frac{b}{2} \right) dxdy \qquad (8)$$

If an axial, inplane load, positive in compression, is applied to the edges of the plate, the potential of this applied load (including the end load on the stiffener) is

$$V = \int_0^L \int_0^b \left[\bar{N}_x u_{,x} + \bar{N}_y v_{,y} + \bar{N}_{xy} (u_{,y} + v_{,x}) \right] dxdy$$

$$+ \int_0^L \int_0^b \frac{\bar{N}_x}{t} (A_s) u_{,x} \delta \left(y - \frac{b}{2} \right) dxdy \qquad (9)$$

However, since in the absence of middle surface stretching ($\epsilon_x = \epsilon_y = \gamma_{xy} = 0$ when $z = 0$), it can be observed from Equation (1) that

$$u_{,x} = -\frac{1}{2} w^2_{,x} \qquad \text{(Continued)}$$

$$v_{,y} = -\frac{1}{2} w_{,y}^2$$

$$u_{,y} + v_{,x} = -w_{,x} w_{,y} \tag{10}$$

Substitution of Equation (10) in Equation (9) yields

$$V = -\frac{1}{2} \int_0^L \int_0^b \left[\bar{N}_x w_{,x}^2 + \bar{N}_y w_{,y}^2 + 2\bar{N}_{xy} w_{,x} w_{,y} + \frac{\bar{N}_x}{t} (A_s) w_{,x}^2 \delta\left(y - \frac{b}{2}\right) \right] dxdy \tag{11}$$

Finally, the total potential is the sum of Equations (6), (8), and (11) and becomes

$$U + V = \frac{1}{2} \int_0^L \int_0^b \left\{ \frac{D_x}{1 - \mu_x \mu_y} w_{,xx}^2 + \frac{D_x \mu_y + D_y \mu_x}{1 - \mu_x \mu_y} w_{,xx} w_{,yy} + \frac{D_y}{1 - \mu_x \mu_y} w_{,yy}^2 + 2D_{xy} w_{,xy}^2 + \left[(EI) w_{,xx}^2 + (GJ) w_{,xy}^2 \right] \delta\left(y - \frac{b}{2}\right) - \bar{N}_x w_{,x}^2 - \bar{N}_y w_{,y}^2 - 2\bar{N}_{xy} w_{,x} w_{,y} - \frac{\bar{N}_x}{t} (A_s) w_{,x}^2 \delta\left(y - \frac{b}{2}\right) \right\} dxdy \tag{12}$$

VARIATIONAL PRINCIPLE AND GOVERNING EQUATIONS

In accordance with the potential energy principle, the total potential, $U + V$, must have a stationary value with respect to admissible variations in the lateral deflection, w, in order for equilibrium to be achieved. This variation leads to the equilibrium or Euler equation

of the variation, plus the applicable boundary conditions. The variation of Equation (12) leads to the following equilibrium equation:

$$\frac{D_x}{1 - \mu_x\mu_y}\left[w_{,xxxx} + \frac{D_y}{D_x} w_{,yyyy} + \left(\mu_y + \mu_x \frac{D_y}{D_x}\right) w_{,xxyy}\right] + 2D_{xy} w_{,xxyy}$$

$$+ \left[(EI)\, w_{,xxxx} + (GJ)\, w_{,xxyy}\right] \delta\left(y - \frac{b}{2}\right) = \bar{N}_x w_{,xx} + \bar{N}_y w_{,yy}$$

$$+ 2\bar{N}_{xy} w_{,xy} + \frac{\bar{N}_x}{t}(A_s)\, w_{,xx}\, \delta\left(y - \frac{b}{2}\right) \qquad (13)$$

The associated boundary conditions for the case of single support are obtained as

$$w = 0 \quad \text{and} \quad -\frac{D_x}{1 - \mu_x\mu_y}\left[w_{,xx} + \mu_y w_{,yy}\right] = M_x = 0 \quad @ \quad x = 0, L$$

$$w = 0 \quad \text{and} \quad -\frac{D_y}{1 - \mu_x\mu_y}\left[w_{,yy} + \mu_x w_{,xx}\right] = M_y = 0 \quad @ \quad y = 0, b \qquad (14)$$

The solution of Equation (13), consistent with the boundary conditions, Equation (14) leads to the deflection function, w . This, however, is a difficult procedure in general and is not the approach followed in this investigation. Rather, the direct method of the calculus of variations (Rayleigh-Ritz method) is used to determine the buckling criteria for w expressed in terms of a series of arbitrary parameters.

METHOD OF SOLUTION

With the total potential energy given by Equation (12) in terms of the plate deflection w, the direct method of the calculus of variations (Rayleigh-Ritz method) is used to determine the minimum buckling load for varying stiffener size and composite content.

GENERAL CASE

A deflection function satisfying the boundary conditions for a flat, simply supported, stiffened rectangular plate under axial compression is

$$w = \sum_{n}^{\infty} A_{mn} \sin \frac{m\pi x}{L} \sin \frac{n\pi y}{b} \quad . \tag{15}$$

Substitution of Equation (15) into Equation (12) (with $\bar{N}_y = \bar{N}_{xy} = 0$) and subsequent integration over the surface of the plate yields (see Appendix I)

$$U + V = \frac{1}{2} \sum_{n}^{\infty} \left\{ \frac{D_x}{1 - \mu_x\mu_y} \left[A_{mn}^2 \left(\frac{m\pi}{L} \right)^4 \frac{Lb}{4} \right] \right.$$

$$+ \frac{D_x\mu_y + D_y\mu_x}{1 - \mu_x\mu_y} \left[A_{mn}^2 \left(\frac{m\pi}{L} \right)^2 \left(\frac{n\pi}{b} \right)^2 \frac{Lb}{4} \right] + \frac{D_y}{1 - \mu_x\mu_y} \left[A_{mn}^2 \left(\frac{n\pi}{b} \right)^4 \frac{Lb}{4} \right]$$

$$\left. + 2D_{xy} \left[A_{mn}^2 \left(\frac{m\pi}{L} \right)^2 \left(\frac{n\pi}{b} \right)^2 \frac{Lb}{4} \right] \right\} + \frac{1}{2} (EI) \left(\frac{m\pi}{L} \right)^4 \frac{L}{2} \left[\sum_{n}^{\infty} A_{mn} \sin \frac{n\pi}{2} \right]^2$$

$$+ \frac{1}{2} (GJ) \left(\frac{m\pi}{L} \right)^2 \frac{L}{2} \left[\sum_{n}^{\infty} \frac{n\pi}{b} A_{mn} \cos \frac{n\pi}{2} \right]^2 \qquad \text{(Continued)}$$

$$- \frac{\bar{N}_x}{2} \sum_n^{\infty} A_{mn}^2 \left(\frac{m\pi}{L}\right)^2 \frac{Lb}{4}$$

$$- \frac{\bar{N}_x(A_s)}{2t} \left(\frac{L}{2}\right)\left[\sum_n^{\infty} A_{mn}\left(\frac{m\pi}{L}\right) \sin\frac{m\pi}{2}\right]^2 \qquad (16)$$

The vanishing of the first variation of the total potential energy with respect to A_{mn}, the nondimensional arbitrary displacement parameter, yields the equilibrium condition and a criterion for obtaining the buckling load. This procedure, as shown in Appendix I, yields

$$A_{mn}\left\{\frac{1}{1-\mu_x\mu_y}\left[1+\left(\mu_y+\frac{D_x}{D_y}\mu_x\right)\alpha^2+\frac{D_y}{D_x}n^4\alpha^4\right]+2\frac{D_{xy}}{D_x}n^2\alpha^2-k_x\alpha^2\right\}$$

$$+\frac{2(EI)}{D_x b}\sin\frac{m\pi}{2}\sum_p^{\infty}A_{mp}\sin\frac{p\pi}{2}$$

$$+\frac{2(GJ)}{D_x b}\left(\frac{b}{m\pi}\right)n^2\alpha^2\cos\frac{m\pi}{2}\sum_p^{\infty}A_{mp}\frac{p\pi}{b}\cos\frac{p\pi}{2}$$

$$-\frac{2(A_s)}{bt}k_x\alpha^2\sin\frac{m\pi}{2}\sum_p^{\infty}A_{mp}\sin\frac{p\pi}{2}=0 \qquad (17)$$

where

$$\alpha = \frac{L}{bm}$$

$$k_x = \frac{\bar{N}_x b^2}{\pi^2 D_x}$$

HOMOGENEOUS, ISOTROPIC SQUARE PLATE

A homogeneous, isotropic square plate with an equivalent stiffener (to account for varying amounts of composite material) has been selected as the specific case for examination in the present investigation. A square plate with one centrally located longitudinal stiffener under these loading conditions would buckle in one of two configurations: (1) one half-wave in each direction $(m = n = 1)$ or, (2) two half-waves in each direction $(m = n = 2)$. Any other combinations of m and n would not lead to the minimum value of the buckling coefficient k_x . As noted from Equation (17) the bending stiffness term $(EI)/Db$ of the stiffener is effective only during the $1,1$ mode, and conversely, the torsional stiffness term $(GJ)/Db$ is effective only during the $2,2$ mode.

For an approximate solution, the first term of the deflection function, Equation (15), could be used. However, this would allow only for a pure sinusoidal half-wave deflection pattern of the plate in the chordwise direction. As stiffener size or stiffness is increased, rotation at the inflection point of the $2,2$ mode is somewhat restrained, indicating the need for at least a two-term deflection function; that is, $n = 1,3$ for the $1,1$ mode and $n = 2,4$ for the $2,2$ mode of Equation (17). The result of carrying out this procedure (see Appendix I) is

$$\left[1 + \frac{4(A_s)}{bt}\right] k_x^2 - 104\left[1 + \frac{2(A_s)}{bt} + \frac{(EI)}{26Db}\right] k_x + 16\left[25 + 13\,\frac{(EI)}{Db}\right] = 0 \qquad (18)$$

for the $1,1$ mode and

$$\frac{k_x^2}{16} - \left[\frac{29}{4} + \frac{5}{2}\,\frac{(GJ)}{Db}\right] k_x + 2\left[50 + 41\,\frac{(GJ)}{Db}\right] = 0 \qquad (19)$$

for the 2,2 mode, where D is the bending rigidity for a homogeneous, isotropic plate. The quantities (EI) and (GJ) are the bending and torsional stiffnesses, respectively, of the equivalent longitudinal stiffener. The procedure for determining these values for varying amounts of composite material in the overall stiffener is given in Appendix II.

The minimum values of k_x may be calculated from Equations (18) and (19) in each of the two modes of the square, stiffened plate for varying values of $(EI)/Db$, $(GJ)/Db$, and $(A_s)/bt$. The critical stress, σ_{cr}, is then calculated from the relationship

$$\sigma_{cr} = \frac{k_x \pi^2 D}{b^2 t} \qquad (20)$$

The average density of the plate-stiffener system is a nondimensional measure of the relative weight of the combination with the introduction of composite materials into the system. This factor is calculated by averaging the densities of the system as follows

$$\rho_{ave} = \rho_{comp} (\% \text{ comp}) + \rho_{base} (\% \text{ base}) \qquad (21)$$

where (% comp) is the percent by volume of composite in the entire plate stiffener system, and (% base) is the percent by volume of the base metal used (aluminum, steel, etc.).

The buckling efficiency of the stiffened plate combination (σ_{cr}/ρ_{ave}) is plotted versus $(A_s)/bt$ for varying amounts (by volume) of composite material in the stiffener in Figures 2 through 4. Aluminum is the base material, with either boron epoxy or graphite epoxy used as the advanced composite material.

Peterson[3] determined that the optimum longitudinal stiffener for a flat plate has the relative proportions (1) stiffener width equal to twice

plate thickness, and (2) stiffener height equal to eight times the plate thickness. These ratios are utilized as starting values for the present investigation.

RESULTS AND DISCUSSION

An investigation of the axial compression buckling of a simply supported flat plate with a central longitudinal stiffener has been undertaken to estimate the effects of composite reinforcement of the stiffener with stiffener torsional stiffness effects included. The minimum or critical values of k_x, using Equations (18) and (19), are calculated for the two modes of a stiffened, square, homogeneous, isotropic plate for varying values of $(EI)/Db$ and plotted in Figure 5. These values are in excellent agreement with those of Seide and Stein[5] for the $m = 1$, $n = 1$ case, but the $\left(k_x\right)_{cr}$ values of this investigation are slightly higher than those of Reference 5 for the $m = 2$, $n = 2$ case. This discrepancy is due to the inclusion of the torsional stiffness of the stiffener in the present analysis. Without torsional stiffness effects, $\left(k_x\right)_{cr}$ for the $m = 2$, $n = 2$ case remains constant at a value of 16 despite the size of the stiffener. Timoshenko and Gere,[8] in the case of a plate simply supported on three edges with one of the unloaded edges clamped under compressive loading show the maximum value of $\left(k_x\right)_{cr}$ to be 22.6. This would be analogous to the present problem when the torsional stiffness is infinitely large. The two-term deflection function used in the present investigation will result in values of $\left(k_x\right)_{cr}$ higher than that arrived at by Reference 8, but only when the stiffener size is excessively large and out of the area of practical interest. Equations (18) and (19) give values of $\left(k_x\right)_{cr}$ which are sufficiently accurate, as the primary aim of the present report is to investigate the trends of plate efficiency rather than to calculate actual design data concerning buckling loads.

The primary quantity for demonstrating plate buckling efficiency in this investigation is σ_{cr}/ρ_{ave}, where σ_{cr} is the critical stress of the plate determined from Equation (20), and ρ_{ave} is the average density determined from Equation (21). Figure 2 is a graph of σ_{cr}/ρ_{ave} for a square aluminum plate with a centrally located longitudinal stiffener augmented by varying amounts of graphite-epoxy composite. The buckling

efficiency has been calculated for varying stiffener size. The sharp knee in each of the curves results from the transition of the plate buckling pattern from a $m = 1$, $n = 1$ configuration to a $m = 2$, $n = 2$ mode. To the left of this knee, or in the 1,1 mode, significant increases in buckling efficiency result from the replacement of aluminum with graphite epoxy in the stiffener. This is due to the increased flexural stiffness of the stiffener, since the graphite epoxy has a greater value of Young's modulus than does aluminum. However, to the right side of the knee, in the 2,2 buckling configuration, the plate buckling efficiency is actually reduced with the addition of the graphite epoxy. Once the 2,2 condition is reached, the stiffener lies at a node of the plate, and the flexural stiffness of the stiffener has no effect on the magnitude of the critical stress. Only the torsional stiffness of the stiffener is a factor in this range and, since the shear modulus of aluminum is approximately three times that of graphite epoxy, the overall buckling efficiency decreases with the addition of the composite material. As an example, a plate with an all-aluminum stiffener and a value of $(A_s)/bt$ of 0.205 attains a buckling efficiency parameter value of 41.0×10^4 in. (Point A). If the aluminum stiffener is then replaced by an all composite stiffener, this parameter value is decreased to 38.8×10^4 in. (Point B).

It may also be noted from Figure 2 that in the 1,1 configuration, as the percentage of composite in the stiffener increases, the percent increase in the buckling efficiency decreases. For a plate with a value of $(A_s)/bt$ of 0.08, σ_{cr}/ρ_{ave} equals 15.7×10^4 in. for an all aluminum stiffener. The replacement of 10 percent of the stiffener cross-section with graphite epoxy raises the value of σ_{cr}/ρ_{ave} to 19.5×10^4 in., a percentage increase of almost 25 percent. Raising the percentage of composite to 50 percent gives a buckling efficiency parameter value of 28.3×10^4 in., or an increase of 80 percent over the all aluminum stiffener. An all composite stiffener has a σ_{cr}/ρ_{ave} value of 31.6×10^4, or a little greater than a 100 percent increase over the metal stiffener. In another case, where the

size of the stiffener is increased to give a value of $(A_s)/bt$ of 0.14 , a 10-percent-composite stiffener has approximately the same value of σ_{cr}/ρ_{ave} as the all-composite stiffener, although the latter structure will be lighter in weight and much higher in cost.

As mentioned previously, past studies having to do with the buckling properties of all-metal stiffened plates have generally neglected the torsional rigidity of the stiffener. Figure 3 is a graph of the same plate-stiffener combination as that of Figure 2; however, the shear modulus of graphite epoxy is assumed to be identical to that of aluminum $(G = 4.0 \times 10^6 \text{ lb/in.}^2)$. In this case, the replacement of a percentage of the aluminum in the stiffener with graphite epoxy always results in an increase in σ_{cr}/ρ_{ave} without regard to the percentage of composite, size of the stiffener, or the buckling pattern of the plate. Thus, it is evident that the torsional stiffness of a reinforced metal stiffener can play a significant role in the stability problem and should not be overlooked when high-extensional modulus composites are introduced to improve structural efficiency.

Another popular composite material in developmental use is boron epoxy. This composite, although having a higher value of Young's modulus, is appreciably more dense and significantly more expensive than graphite epoxy. Figure 4 is a plot of the buckling efficiency of a boron-epoxy-augmented stiffened plate. Comparison of Figure 4 with Figure 2 reveals that although the use of boron epoxy results in higher values of σ_{cr}/ρ_{ave} than graphite epoxy in the 1,1 buckling configuration, it results in greater loss in efficiency when in the 2,2 mode. Higher values of σ_{cr}/ρ_{ave} in the 1,1 mode are the result of the increased Young's modulus for boron epoxy, whereas the reduced efficiency in the 2,2 configuration is attributed to the increased weight of boron epoxy and the fact that the shear moduli of the two materials are essentially the same.

CONCLUDING REMARKS

This investigation develops a buckling criterion for axially compressed, simply supported, flat, rectangular, homogeneous, isotropic plates with composite-reinforced, centrally located, longitudinal stiffeners. This criterion is obtained from a more general development based on orthotropic plate theory. Comparison of the results of the present study with past investigations shows the derived buckling coefficient to be generally more realistic than those which neglect the torsional stiffness of the stiffener when the plate cross-section aspect ratio between stiffeners is at least sixty or less.

It is also shown that the addition of composites to improve the efficiency of a stiffened flat plate requires more judicious consideration than simply replacing conventional material with high-performance fibrous composites. Effects which may have proved to be negligible in the analysis of conventional structures can become significant in the conventional-composite combination due to the relatively large spread between E and G in advanced composites as compared with that in conventional metals. The replacement of a conventional stiffener with one consisting of composites will usually lead to lighter structural weight, but the undesirable side effects of lower buckling efficiency and increased cost may also be introduced. Careful study must be made as to the amount of composite to be used, the percentage of increase in buckling efficiency actually achieved, and the additional costs involved. It has been shown that in certain cases, a rather minimal use of composites will result in maximum gain in weight reduction and increase in critical stress with relatively small increases in cost.

When working with advanced composites, the designer of high-performance vehicles can no longer neglect the torsional rigidity of a stiffener as was normally done with low subsonic-range all-metal systems. Such neglect can introduce errors which may tend to show that any use of composites will achieve additional gains in structural efficiency, when in fact this is not so. The lower shear modulus of composites requires that

the effects of torsional rigidity should always be taken into account, as unconservative errors in critical stress may result in either premature buckling or reduced buckling efficiency.

The designer must also be cognizant of all the advantages and disadvantages of the various composite materials now becoming available. As shown herein for graphite and boron epoxy, each of these materials has certain advantages, and the most suitable material must be chosen for the specific application at hand. Composite materials present the possibility of increased strength and stiffness along with decreases in structural weight, but careful study must be made with regard to proper use and material selectivity to achieve optimized structural efficiency and fabricability at minimum cost.

REFERENCES

1. Arvin, G. H., STRUCTURAL DESIGN GUIDE FOR ADVANCED COMPOSITE APPLICATIONS, prepared for U.S.A.F. Materials Laboratory by Los Angeles Division of North American Rockwell, August 1969, pp. 1.6.1-1.6.3.

2. Durlofsky, H., and Mayers, J., EFFECTS OF INTERLAMINAR SHEAR ON THE BENDING AND BUCKLING OF LAMINATED BEAMS, Stanford University; USAAVLABS Technical Report 70-7, U.S. Army Aviation Materiel Laboratories, Fort Eustis, Virginia, March 1970.

3. Peterson, J. P., STRUCTURAL EFFICIENCY OF ALUMINUM MULTIWEB BEAMS AND Z-STIFFENED PANELS REINFORCED WITH FILAMENTARY BORON-EPOXY COMPOSITE, NASA Technical Note D-5856, National Aeronautics and Space Administration, June 1970.

4. Barbré, R., STABILITY OF RECTANGULAR PLATES WITH LONGITUDINAL OR TRANSVERSE STIFFENERS UNDER UNIFORM COMPRESSION, NACA Technical Memorandum 904, National Advisory Committee for Aeronautics, August 1939.

5. Seide, P., and Stein, M., COMPRESSIVE BUCKLING OF SIMPLY SUPPORTED PLATES WITH LONGITUDINAL STIFFENERS, NACA Technical Note 1825, National Advisory Committee for Aeronautics, 1949.

6. Gomza, A., and Stein, M., MINIMUM-WEIGHT DESIGN OF SIMPLY SUPPORTED TRANSVERSELY STIFFENED PLATES UNDER COMPRESSION, NACA Technical Note 1710, National Advisory Committee for Aeronautics, September 1948.

7. Mayers, J., and Wesenberg, D. L., THE MAXIMUM STRENGTH OF INITIALLY IMPERFECT, AXIALLY COMPRESSED, CIRCULAR CYLINDRICAL SHELLS, Stanford University; USAAVLABS Technical Report 69-60, U.S. Army Aviation Materiel Laboratories, Fort Eustis, Virginia, August 1969.

8. Timoshenko, S., and Gere, J. M., THEORY OF ELASTIC STABILITY, Second Edition, McGraw Hill Book Co., Inc., 1961, pp. 367-370.

9. Timoshenko, S., and Young, D. H., ELEMENTS OF STRENGTH OF MATERIALS, Fourth Edition, Van Nostrand Co., Inc., 1962, pp. 72, 145-148.

10. Timoshenko, S., and Goodier, J. N., THEORY OF ELASTICITY, Second Edition, McGraw Hill Book Co., Inc., 1951, pp. 277-278.

APPENDIX I

DEVELOPMENT OF BUCKLING CRITERION

The total potential energy, Equation (12) (with $\bar{N}_y = \bar{N}_{xy} = 0$), upon substitution of the deflection function, Equation (15), yields

$$
\begin{aligned}
U + V = \frac{1}{2} \int_0^L \int_0^b \Bigg\{ & \frac{D_x}{1 - \mu_x \mu_y} \left[- \sum_n^\infty A_{mn} \left(\frac{m\pi}{L} \right)^2 \sin \frac{m\pi x}{L} \sin \frac{n\pi y}{b} \right]^2 \\
& + \frac{D_x \mu_y + D_y \mu_x}{1 - \mu_x \mu_y} \left[- \sum_n^\infty A_{mn} \left(\frac{m\pi}{L} \right)^2 \sin \frac{m\pi x}{L} \sin \frac{n\pi y}{b} \right] \\
& \times \left[- \sum_n^\infty A_{mn} \left(\frac{n\pi}{b} \right)^2 \sin \frac{m\pi x}{L} \sin \frac{n\pi y}{b} \right] \\
& + \frac{D_y}{1 - \mu_x \mu_y} \left[- \sum_n^\infty A_{mn} \left(\frac{n\pi}{b} \right)^2 \sin \frac{m\pi x}{L} \sin \frac{n\pi y}{b} \right]^2 \\
& + 2D_{xy} \left[\sum_n^\infty A_{mn} \left(\frac{m\pi}{L} \right) \left(\frac{n\pi}{b} \right) \cos \frac{m\pi x}{L} \cos \frac{n\pi y}{b} \right]^2 \\
& + (EI)\, \delta \left(y - \frac{b}{2} \right) \left[- \sum_n^\infty A_{mn} \left(\frac{m\pi}{L} \right)^2 \sin \frac{m\pi x}{L} \sin \frac{n\pi y}{b} \right]^2 \\
& + (GJ)\, \delta \left(y - \frac{b}{2} \right) \left[\sum_n^\infty A_{mn} \left(\frac{m\pi}{L} \right) \left(\frac{n\pi}{b} \right) \cos \frac{m\pi x}{L} \cos \frac{n\pi y}{b} \right]^2 \\
& - \bar{N}_x \left[\sum_n^\infty A_{mn} \left(\frac{m\pi}{L} \right) \cos \frac{m\pi x}{L} \sin \frac{n\pi y}{b} \right]^2 \qquad \text{(Continued)}
\end{aligned}
$$

$$- \frac{\bar{N}_x(A_s)}{t} \delta\left(y - \frac{b}{2}\right)\left[\sum_n^{\infty} A_{mn}\left(\frac{m\pi}{L}\right) \cos\frac{m\pi x}{L} \sin\frac{m\pi y}{b}\right]^2 \Bigg\} dxdy \tag{22}$$

Integration of this expression over the area of the plate yields

$$\begin{aligned} U + V = \frac{1}{2} \sum_n^{\infty} \Bigg\{ & \frac{D_x}{1 - \mu_x\mu_y}\left[A_{mn}^2\left(\frac{m\pi}{L}\right)^4 \frac{Lb}{4}\right] \\ & + \frac{D_x\mu_y + D_y\mu_x}{1 - \mu_x\mu_y}\left[A_{mn}^2\left(\frac{m\pi}{L}\right)^2\left(\frac{m\pi}{2}\right)^2 \frac{Lb}{4}\right] \\ & + \frac{D_y}{1 - \mu_x\mu_y}\left[A_{mn}^2\left(\frac{m\pi}{b}\right)^4 \frac{Lb}{4}\right] + 2D_{xy}\left[A_{mn}^2\left(\frac{m\pi}{L}\right)^2\left(\frac{m\pi}{b}\right)^2 \frac{Lb}{4}\right]\Bigg\} \\ & + \frac{1}{2}\Bigg\{(EI)\left(\frac{L}{2}\right)\left(\frac{m\pi}{L}\right)^4\left[\sum_n^{\infty} A_{mn} \sin\frac{m\pi}{2}\right]^2 \\ & + (GJ)\left(\frac{L}{2}\right)\left(\frac{m\pi}{L}\right)^2\left[\sum_n^{\infty}\left(\frac{m\pi}{b}\right) A_{mn} \cos\frac{m\pi}{2}\right]^2 \\ & - \bar{N}_x\left[\sum_n^{\infty} A_{mn}^2\left(\frac{m\pi}{L}\right)^2 \frac{Lb}{4}\right] \\ & - \frac{\bar{N}_x(A_s)}{t}\left(\frac{L}{2}\right)\left[\sum_n^{\infty} A_{mn}\left(\frac{m\pi}{L}\right) \sin\frac{m\pi}{2}\right]^2\Bigg\} \end{aligned} \tag{23}$$

Now, the first variation of Equation (23) with respect to A_{mn} must reduce to zero since any first order change in the total potential must vanish for every admissible variation in the lateral displacement

function. Hence,

$$A_{mn}\left\{\left[\frac{D_x}{1-\mu_x\mu_y}\left(\frac{m\pi}{L}\right)^4+\frac{D_x\mu_y+D_y\mu_x}{1-\mu_x\mu_y}\left(\frac{m\pi}{L}\right)^2\left(\frac{n\pi}{b}\right)^2\right.\right.$$

$$\left.\left.+\frac{D_y}{1-\mu_x\mu_y}\left(\frac{n\pi}{b}\right)^4+2D_{xy}\left(\frac{m\pi}{L}\right)^2\left(\frac{n\pi}{b}\right)^2\right]\frac{Lb}{4}\right\}$$

$$+\left[(EI)\left(\frac{m\pi}{L}\right)^4\left(\frac{L}{2}\right)\sin\frac{n\pi}{2}\sum_p^\infty A_{mp}\sin\frac{p\pi}{2}\right]$$

$$+\left[(GJ)\left(\frac{m\pi}{L}\right)^2\left(\frac{n\pi}{b}\right)\left(\frac{L}{2}\right)\cos\frac{n\pi}{2}\sum_p^\infty A_{mp}\left(\frac{p\pi}{b}\right)\cos\frac{p\pi}{2}\right]$$

$$-\bar{N}_x\left[A_{mn}\left(\frac{m\pi}{L}\right)^2\left(\frac{Lb}{4}\right)\right]$$

$$-\frac{\bar{N}_x(A_s)}{t}\left[\left(\frac{m\pi}{L}\right)^2\left(\frac{L}{2}\right)\sin\frac{n\pi}{2}\sum_p^\infty A_{mp}\sin\frac{p\pi}{2}\right]=0 \qquad (24)$$

Equation (24) reduces to Equation (17) when a factor of $m^4\pi^4bD_x/4L^3$ is removed. For the special case of an isotropic square plate

$$D_x = D_y = D(1-\mu^2)$$

$$D_{xy} = D(1-\mu) \qquad (25)$$

$$\mu_x = \mu_y = \mu$$

Substitution of Equation (25) into Equation (17) yields

$$A_{mn}\left[\left(1 + n^2\alpha^2\right)^2 - k_x\alpha^2\right] + \frac{2(EI)}{Db}\sin\frac{n\pi}{2}\sum_{n}^{\infty} A_{mp}\sin\frac{p\pi}{2}$$

$$+ \frac{2(GJ)}{Db}\left(\frac{b}{n\pi}\right) n^2\alpha^2\cos\frac{n\pi}{2}\sum_{p}^{\infty} A_{mp}\left(\frac{p\pi}{b}\right)\cos\frac{p\pi}{2}$$

$$- \frac{2(A_s)}{bt} k_x\alpha^2 \sin\frac{n\pi}{2}\sum_{p}^{\infty} A_{mp}\sin\frac{p\pi}{2} = 0 \qquad (26)$$

A second approximation solution of Equation (26) for the one half-wave pattern in each direction yields two equations in two unknowns: namely

$$n = 1 \;:\; A_{m1}(4 - k_x) + \frac{2(EI)}{Db}(A_{m1} - A_{m3}) - \frac{2(A_s)}{bt} k_x (A_{m1} - A_{m3}) = 0$$

$$n = 3 \;:\; A_{m3}(100 - k_x) - \frac{2(EI)}{Db}(A_{m1} - A_{m3}) + \frac{2(A_s)}{bt} k_x (A_{m1} - A_{m3}) = 0 \qquad (27)$$

Now, for the A_{mn}'s to possess other than trivial values, the determinant formed by the coefficients of the A_{mn}'s must vanish. Hence,

$$\begin{vmatrix} 4 - k_x + \frac{2(EI)}{Db} - \frac{2(A_s)}{bt} k_x & -\frac{2(EI)}{Db} + \frac{2(A_s)}{bt} k_x \\ -\frac{2(EI)}{Db} + \frac{2(A_s)}{bt} k_x & 100 - k_x + \frac{2(EI)}{Db} - \frac{2(A_s)}{bt} k_x \end{vmatrix} = 0 \tag{28}$$

The solution of this determinant yields Equation (18). The second-approximation solution of Equation (26) for the two half-wave pattern in each direction yields

$$\begin{aligned} n = 2 \quad &: \quad A_{m2}\left(4 - \frac{k_x}{4}\right) + \frac{2(GJ)}{Db}\left(A_{m2} - 2A_{m4}\right) = 0 \\ n = 4 \quad &: \quad A_{m4}\left(24 - \frac{k_x}{4}\right) - \frac{8(GJ)}{Db}\left(\frac{A_{m2}}{2} - A_{m4}\right) = 0 \end{aligned} \tag{29}$$

It follows from the same argument as before that for a solution;

$$\begin{vmatrix} 4 + \frac{2(GJ)}{Db} - \frac{k_x}{4} & -\frac{4(GJ)}{Db} \\ -\frac{4(GJ)}{Db} & 25 + \frac{8(GJ)}{Db} - \frac{k_x}{4} \end{vmatrix} = 0 \tag{30}$$

The solution of Equation (30) yields the result given in Equation (19).



APPENDIX II

DETERMINATION OF EQUIVALENT VALUES OF (EI) AND (GJ) IN COMPOSITE-REINFORCED STIFFENER

Timoshenko and Young[9] describe a common method of transforming a composite beam into an equivalent beam of one material for the determination of bending stiffness. This is done by multiplying the width of the composite section of the stiffener by the ratio of the Young's moduli; that is

$$w_1 = \frac{E_{comp}}{E_{base}} w_2 \tag{31}$$

where w_1 is the original width of the stiffener, and w_2 is the modified width of the composite section of the equivalent stiffener. As an example, suppose $E_{comp} = 3E_{base}$. Then, as shown in Figure 6, the equivalent stiffener would consist of one material, the basic metal, but it would possess a different shape. The moment of inertia of the equivalent stiffener is then found and multiplied by E_{base}, to give the equivalent value of (EI) for the stiffener.

Timoshenko and Goodier[10] give a formula for the twisting moment or torque of a rectangular beam in torsion as

$$T = \frac{1}{3} G\theta (w_1)^3 h \left[1 - \frac{192}{\pi^5} \frac{w_1}{h} \sum_{k=odd}^{\infty} \frac{1}{k^5} \tanh \frac{k\pi h}{2w_1} \right] \tag{32}$$

However, from Reference 9, the torsional stiffness of a beam in free torsion is known to be

$$J = \frac{T}{G\theta} \tag{33}$$

Substitution of Equation (32) into Equation (33) yields

$$J = \frac{1}{3} (w_1)^3 h \left[1 - \frac{192}{\pi^5} \frac{w_1}{h} \sum_{k=odd}^{\infty} \frac{1}{k^5} \tanh \frac{k\pi h}{2w_1} \right] \qquad (34)$$

This value is calculated for each section of the stiffener and multiplied by its respective shear modulus. Addition of these components gives the equivalent (GJ) of the stiffener.

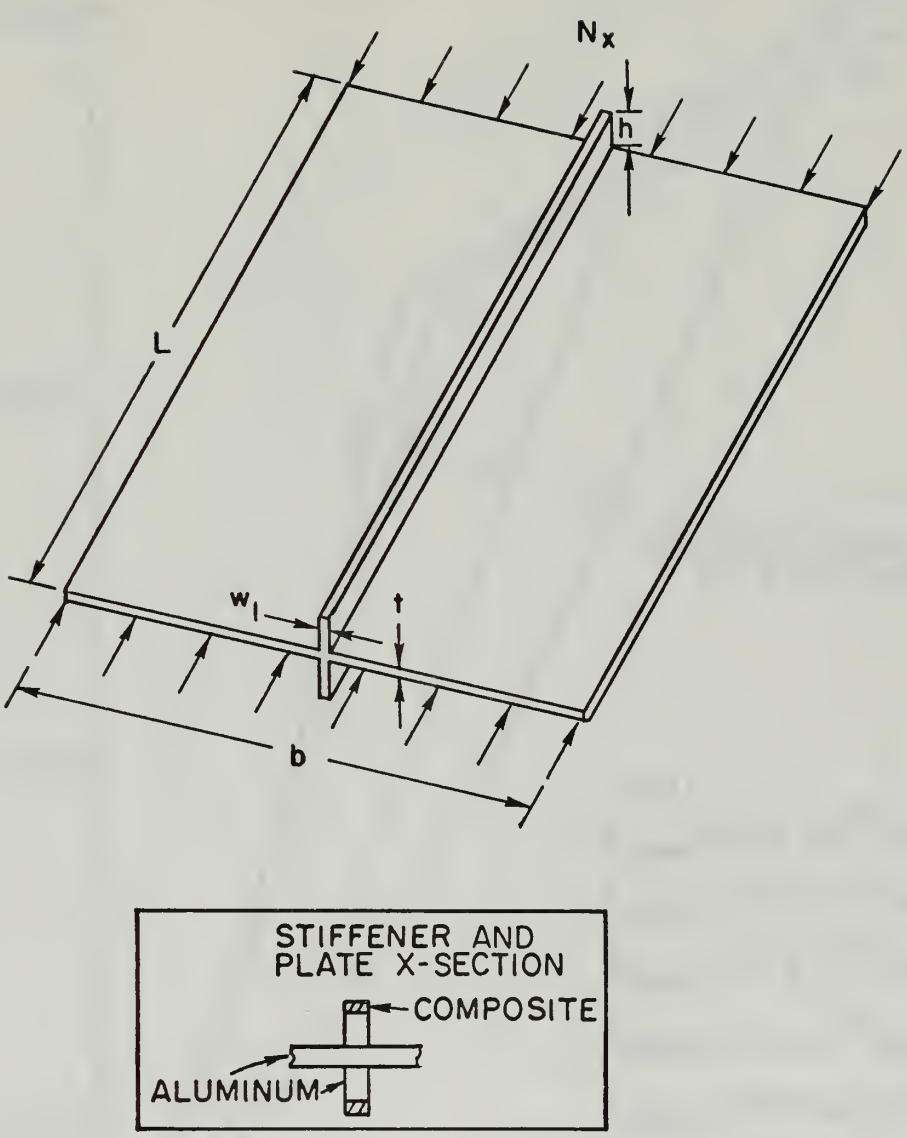


Figure 1. Geometry of Homogeneous, Isotropic Plate With Longitudinal Stiffener.



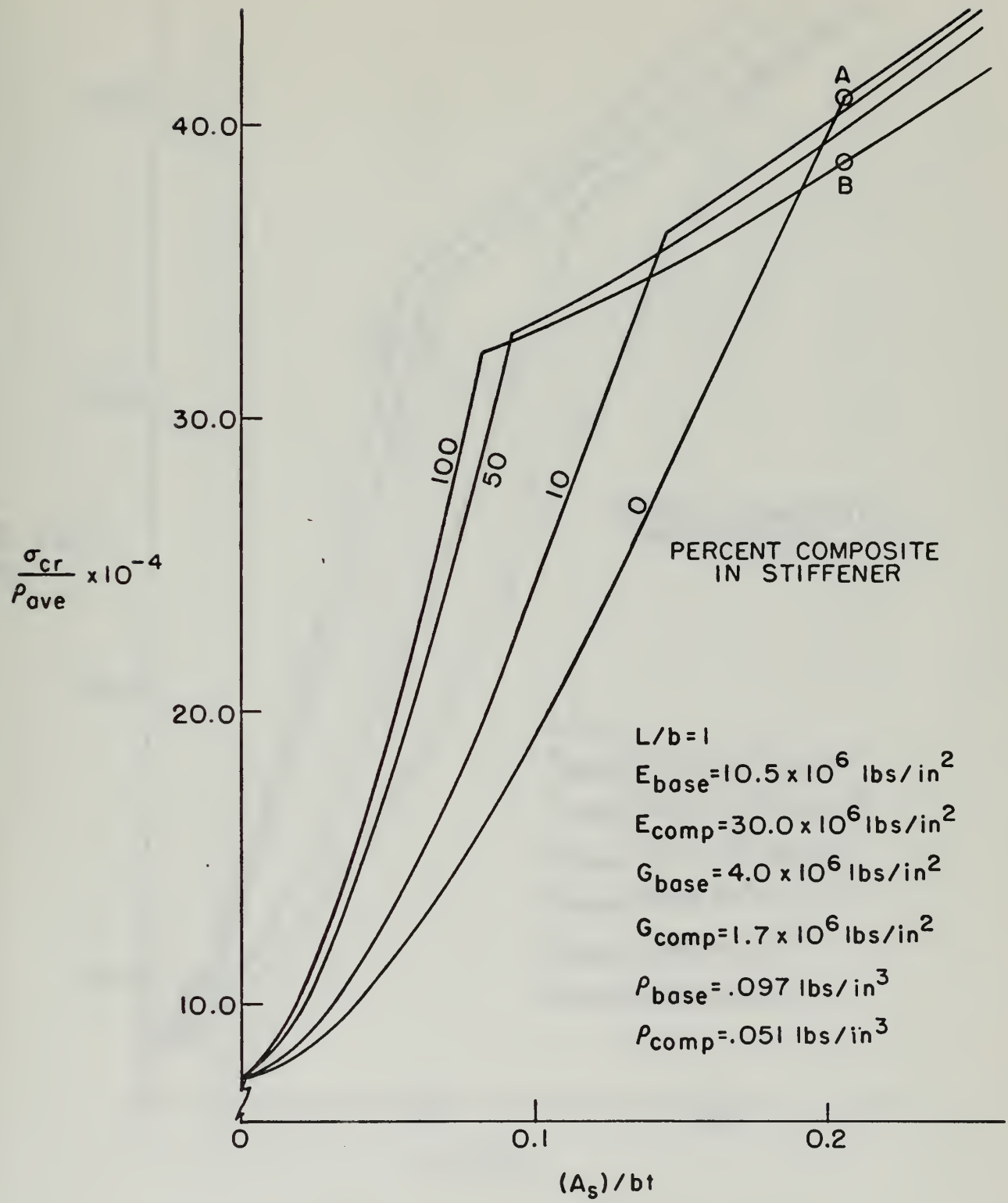


Figure 2. Buckling Efficiency Curve for Aluminum Plate With Longitudinal Stiffener Augmented With Varying Percentage (by Volume) of Graphite Epoxy.



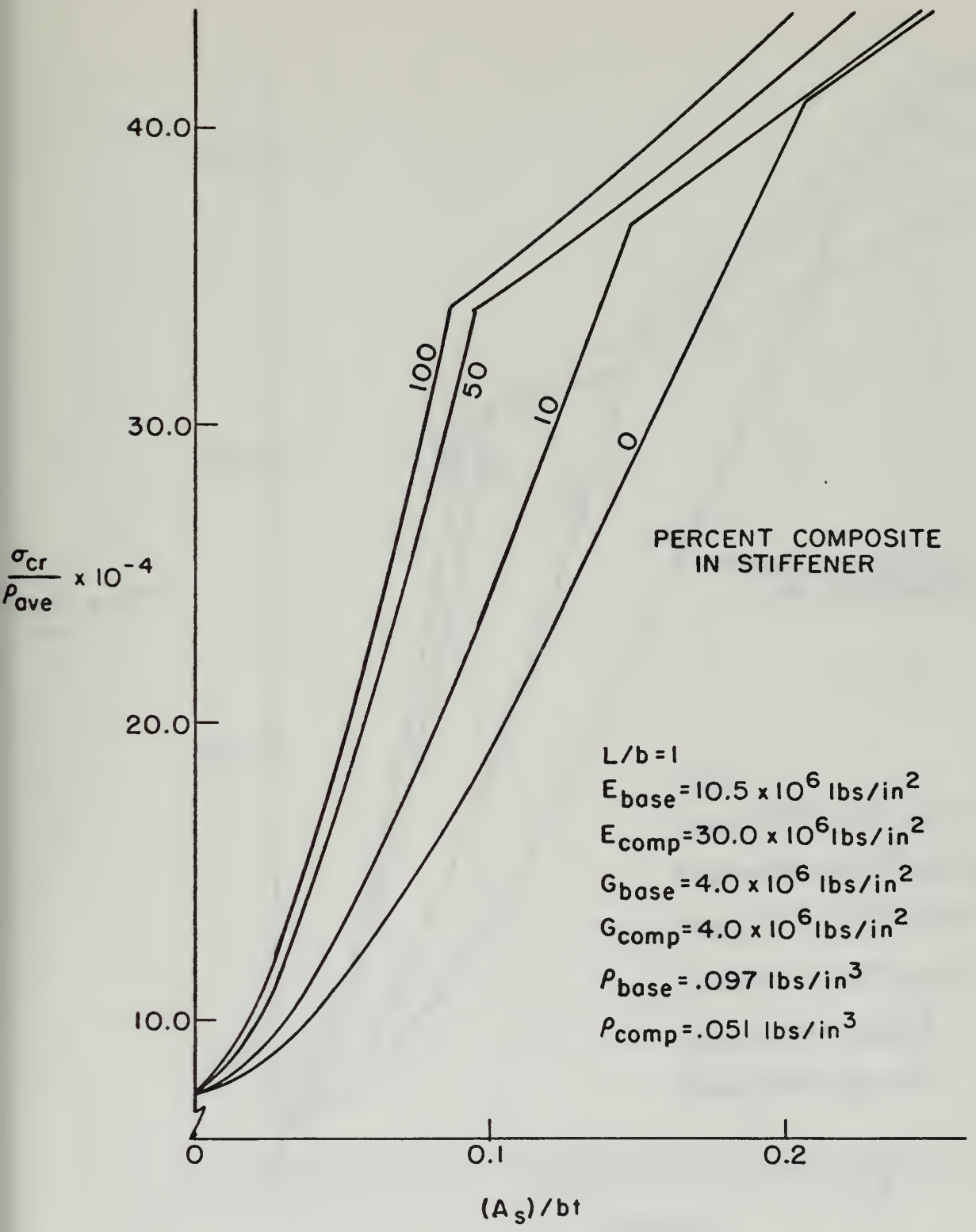


Figure 3. Buckling Efficiency Curve for Aluminum Plate With Longitudinal Stiffener Augmented With Varying Percentage (by Volume) of Graphite Epoxy ($G_{comp} = G_{base}$).



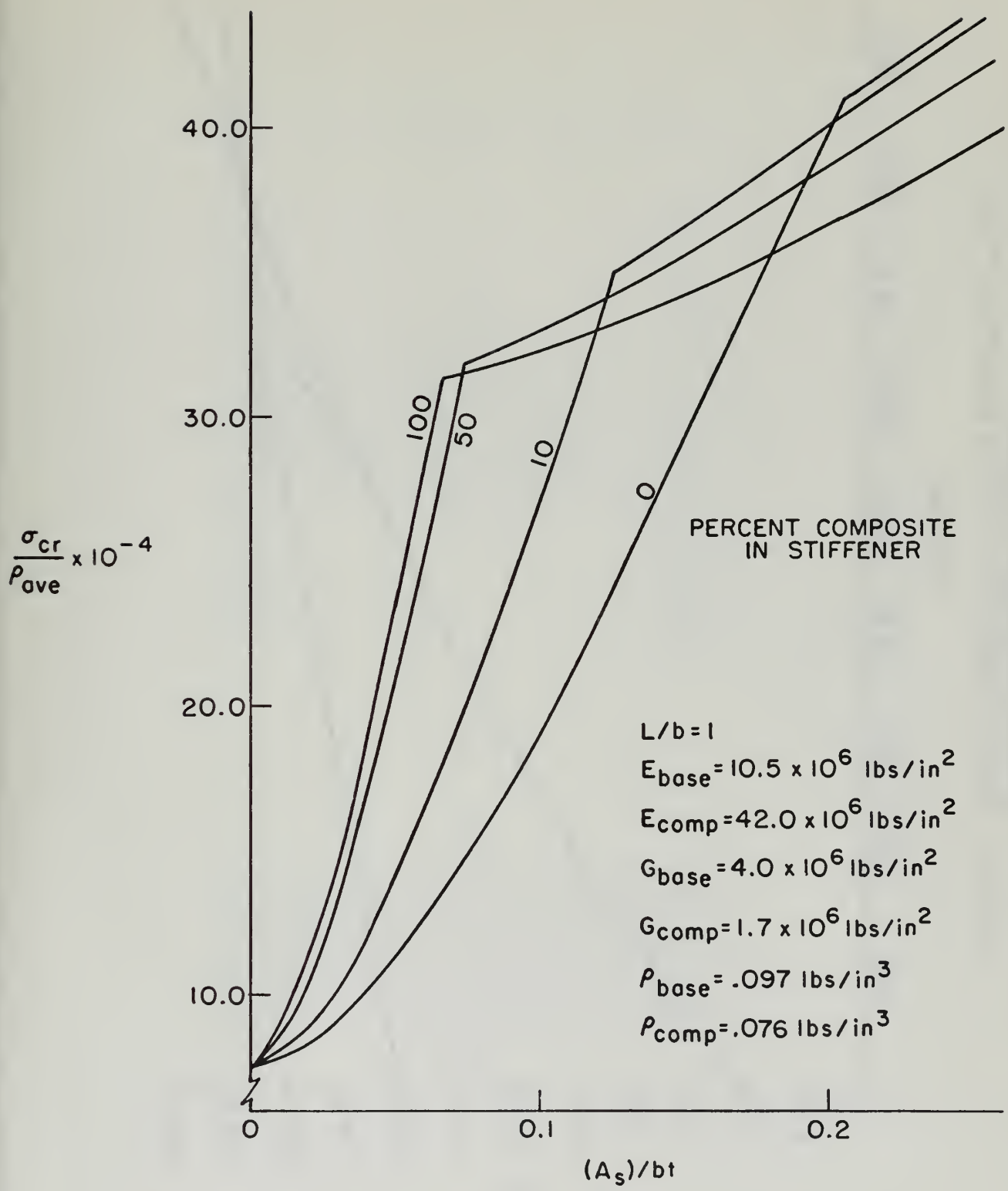


Figure 4. Buckling Efficiency Curve for Aluminum Plate With Longitudinal Stiffener Augmented With Varying Percentage (by Volume) of Boron Epoxy.



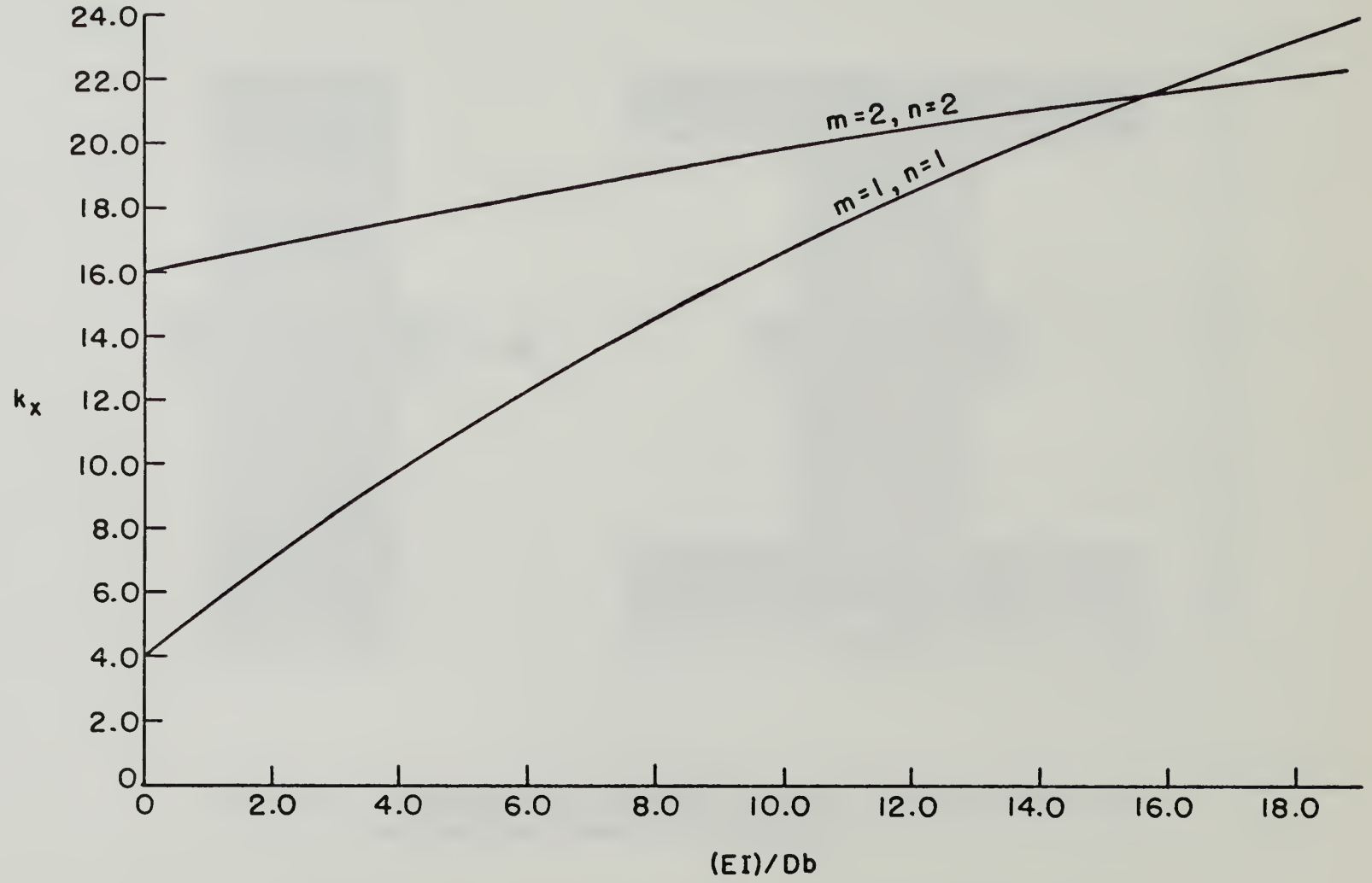


Figure 5. Buckling Coefficient Curve for Aluminum Plate With Aluminum Longitudinal Stiffener.



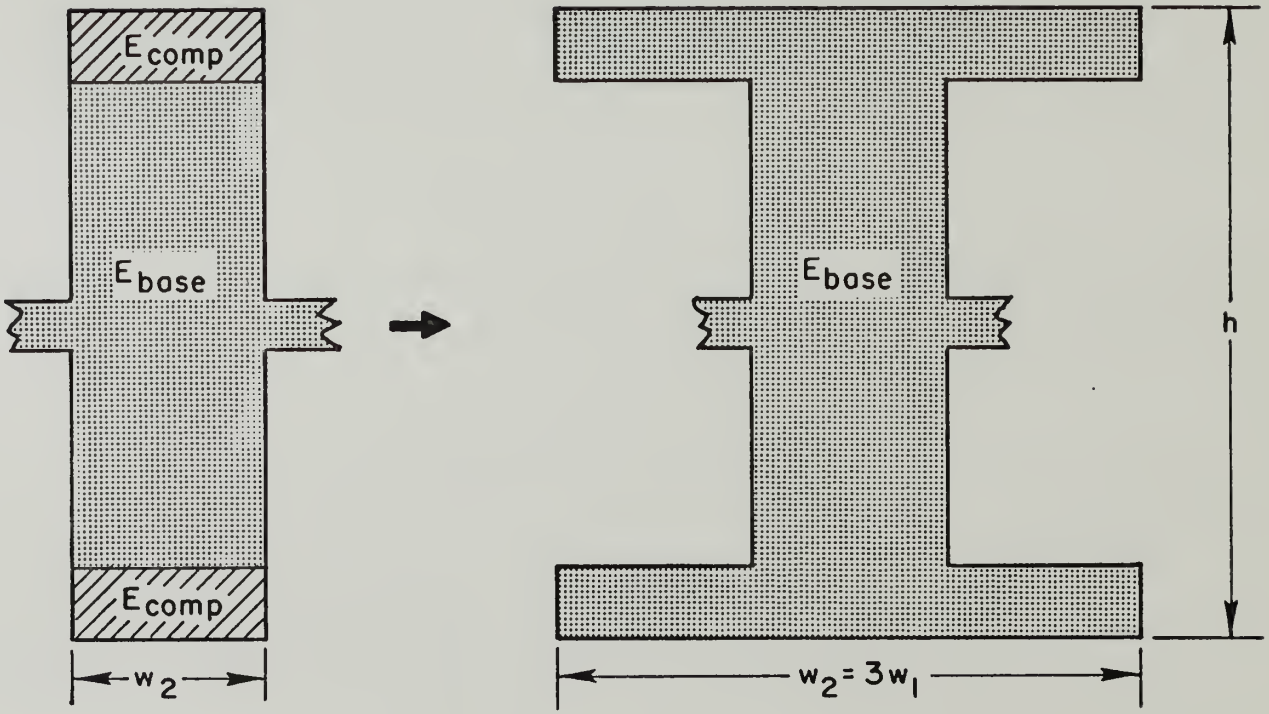


Figure 6. Geometry of the Transformation of a Composite Beam Into an Equivalent Beam of One Material.



132339

Thesis
H9574 Huss

On the compressive buckling of rectangular plates with advanced-composite-reinforced, central longitudinal stiffeners.

132339

Thesis
H9574 Huss

On the compressive buckling of rectangular plates with advanced-composite-reinforced, central longitudinal stiffeners.

thesH9574
On the compressive buckling of rectangul
3 2768 002 13291 2
DUDLEY KNOX LIBRARY